



Diamond nanofocusing refractive X-ray lenses made by planar etching technology

Mikhail Lyubomirskiy,^{a,*} Pit Boye,^b Jan M. Feldkamp,^b Jens Patommel,^b Sebastian Schoeder,^c Andreas Schropp,^a Manfred Burghammer,^d Christoph Wild^e and Christian G. Schroer^{a,f}

Received 18 December 2018

Accepted 16 May 2019

Edited by A. Momose, Tohoku University, Japan

Keywords: diamond; X-ray lenses; compound refractive lens (CRL); focusing.

^aDeutsches Elektronen-Synchrotron DESY, Notkestraße 85, 22607 Hamburg, Germany, ^bInstitute of Structural Physics, TU Dresden, Zellescher Weg 16, 01069 Dresden, Germany, ^cSynchrotron SOLEIL, L'Orme des Merisiers, Saint-Aubin, BP 48, 91192 Gif-sur-Yvette Cedex, France, ^dEuropean Synchrotron Radiation Facility, 71 Avenue des Martyrs, 38043 Grenoble, France, ^eDiamond Materials GmbH, Hans-Bunte-Straße 19, 79108 Freiburg, Germany, and

^fDepartment Physik, Universität Hamburg, Luruper Chaussee 149, 22761 Hamburg, Germany.

*Correspondence e-mail: mikhail.lyubomirskiy@desy.de

The manufacturing steps and first tests of a refractive lens made of polycrystalline diamond are described. A fabrication process based on electron-beam lithography and deep reactive ion etching is introduced. Experimental tests on beamline ID13 at the ESRF have been performed. A spot size of 360 nm (FWHM) at an energy $E = 24.3$ keV is observed.

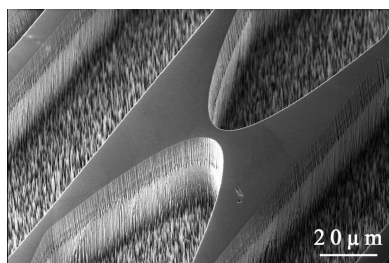
1. Introduction

During recent decades the spectral brightness of X-ray sources has increased significantly, in particular of synchrotron radiation sources and X-ray free-electron lasers (XFELs). In parallel, great advances have been made in the field of X-ray optics, strongly pushing the field of X-ray microscopy and nanoanalysis. In particular, refractive X-ray optics have been developing quickly from the first demonstration experiments (Snigirev *et al.*, 1996) to a widely used optics (Lyubomirskiy & Schroer, 2016).

While lenses made of beryllium are very efficient and widely used, their numerical aperture and thus their minimal focal spot size are limited by the fabrication process. Optics with shorter focal length and thus high numerical aperture can so far only be made of silicon and are far less efficient (Schroer *et al.*, 2003, 2005; Patommel *et al.*, 2017). Diamond, as a low- Z material with high density (3.51 g cm^{-3}), is ideal for efficiently reaching the smallest foci (Schroer & Lengeler, 2005). In addition, thermally resistant refractive lenses are in high demand for future ultra-low-emittance storage rings (Hettel, 2014; Tavares *et al.*, 2014; Schroer *et al.*, 2018) and XFELs.

Looking at the materials pool (Serebrennikov *et al.*, 2016), it is relatively easy to conclude that the most promising lens material is diamond. Being one of the best heat conductors, diamond also has a relatively strong refraction due to its high density. Refractive lenses made of diamond thus have a very large refractive power per unit length. Moreover, compared with silicon, the transmission of diamond is much higher, and only slightly lower than that of Be. Both facts together result in a large numerical aperture (NA) for lenses made of diamond (Schroer *et al.*, 2003).

To date, one can distinguish two branches in the manufacture of diamond optics, deposition and structuring. Deposition is historically the premier approach for manu-



facturing diamond refractive lenses, since there are many challenges in the structuring of diamond and because of the wide availability of well established Si structuring techniques. Because of this the first diamond lens was manufactured by chemical vapour deposition (CVD) of diamond onto an Si matrix and subsequent wet etching of the Si (Snigirev *et al.*, 2002). The matrix was prepared by electron-beam lithography followed by deep anisotropic dry etching (the Bosch process; Bhardwaj & Ashraf, 1995). Those lenses demonstrated a focal spot of micrometre size. Due to the well developed Si deep etching technique, this approach provides a relatively smooth surface of the lens defined by the high-quality silicon template rather than by the diamond deposition. Moreover, the record in focal spot size of diamond lenses has been achieved by this particular approach: 210 nm (Fox *et al.*, 2014). Although a significant success in the competition for focal spot size, one can find a disadvantage in this approach: due to the small feature sizes of the lens shape, especially at the apex of the parabola, CVD is unable to provide a single-crystalline structure of diamond. Furthermore, the authors achieved the smallest focal spot on so-called nanocrystalline diamond lenses (Fox *et al.*, 2014). As a consequence, these lenses have a lower gain (in comparison with single-crystalline lenses) caused by scattering by the grains of the lens material and extinction contrast. The lack of intensity in the focal spot outweighs all the advantages of using diamond as a material for nanofocusing lenses. This seems to be a limiting factor for the use of polycrystalline diamond lenses for flux-hungry applications. In the light of this, structuring seems to be promising, as it allows lenses to be structured out of single-crystalline materials.

To date, there are two known structuring techniques for the manufacturing of diamond lenses: etching and laser ablation. Unfortunately, neither is well developed; the very first lenses etched in diamond demonstrated a focal spot of 3 μm (Nöhammer *et al.*, 2003) and the current record is not significantly better, the smallest achieved spot size at the moment being 1 μm (Isakovic *et al.*, 2009). At the same time, laser ablation also results in a rough surface of the lens, which also makes it impossible to go beyond micrometre focusing (Poli-karpov *et al.*, 2015).

Our target is to elaborate the etching approach in order to achieve sub-100 nm focusing with planar diamond lenses with the highest gain value. In this article, we describe the manufacturing steps and the results of the first experimental tests of nanofocusing diamond planar refractive lenses made of CVD diamond by means of an anisotropic etching technique. For this first attempt we choose a polycrystalline substrate, as single-crystalline wafers are much smaller and much more expensive.

2. Lens manufacture and testing

The main fabrication process steps for the lenses are electron-beam lithography and subsequent deep reactive ion etching. For the structuring process of diamond lenses a high aspect ratio of etching depth to structure width is necessary. We used

different substances as mask materials for the deep reactive ion etching of diamond. For the first prototypes, titanium (Ti) and later tungsten (W) were used. These metallic masks also have to be structured by dry etching processes. For this we used a gold mask manufactured by electron-beam lithography and a lift-off process. The detailed process parameters will be described in the following.

We start with a 300–400 μm -thick polycrystalline diamond wafer made by chemical vapour deposition. The internal structure of the wafer consisted of grains of columnar shape, and their width at the surface plane was estimated to be 60 μm . The wafer was coated with a 500 nm tungsten layer, which serves as a mask for the etching of the lens structures into the diamond. Subsequently, the wafer was spin-coated with a positive electron-beam resist based on polymethylmethacrylate (PMMA). The coated wafer was structured by electron-beam lithography and developed. Afterwards, the lens patterns were transferred into a 100 nm-thick gold layer by gold deposition and lift off. The gold layer was used to pattern the tungsten layer using an SF₆ plasma in an etching tool from SENTECH instruments. The structured tungsten layer served as a hard mask in the deep reactive ion etching (RIE) process of diamond where an oxygen-based plasma was used. Since RIE is not affected by the crystalline structure of the material, similar results can be expected with a single-crystalline wafer. A lens depth of approximately 30 μm was achieved (see Fig. 1).

With the aim of expanding the applicability of a lens chip for a wide range of energies, we structured four different blocks of lenses in a row, each with different radii of curvature of the lenses. Each block holds $N = 100$ lenses with a given curvature and each lens row has corrections in five steps of 200 nm for shape displacement of the fabrication process [for details of corrections see, for instance, Kurapova *et al.* (2007)]. The radius of curvature R lies between 5 μm and 8 μm with 1 μm steps. The proper lens set suitable for the desired energy can be selected by parallel displacement of the chip across the beam.

The performance of the lenses was tested on beamline ID13 at the European Synchrotron Radiation Facility (ESRF). The experimental scheme is presented in Fig. 2. A channel-cut Si(111) monochromator was used to select the desired X-ray energy of $E = 24.3$ keV from a beam produced by the undulator. The lenses were mounted at a distance of $L = 96$ m from the source and aligned in the beam using translation and rotation stages. A platinum pinhole with diameter of 10 μm was situated downstream of the lenses to clean the beam of scattered radiation. The effective source size s was approximately 160 $\mu\text{m} \times 60 \mu\text{m}$ (FWHM) in the horizontal and vertical directions, respectively. The focal length f of a compound lens is given by (Snigirev *et al.*, 1996)

$$f = R/(2N\delta), \quad (1)$$

where R is the radius of curvature of the individual lens surfaces, δ is the real part of the refractive index decrement and N is the number of doubly curved lenses in a stack. In our case, for a lens row with a radius of curvature of $R = 6 \mu\text{m}$, the

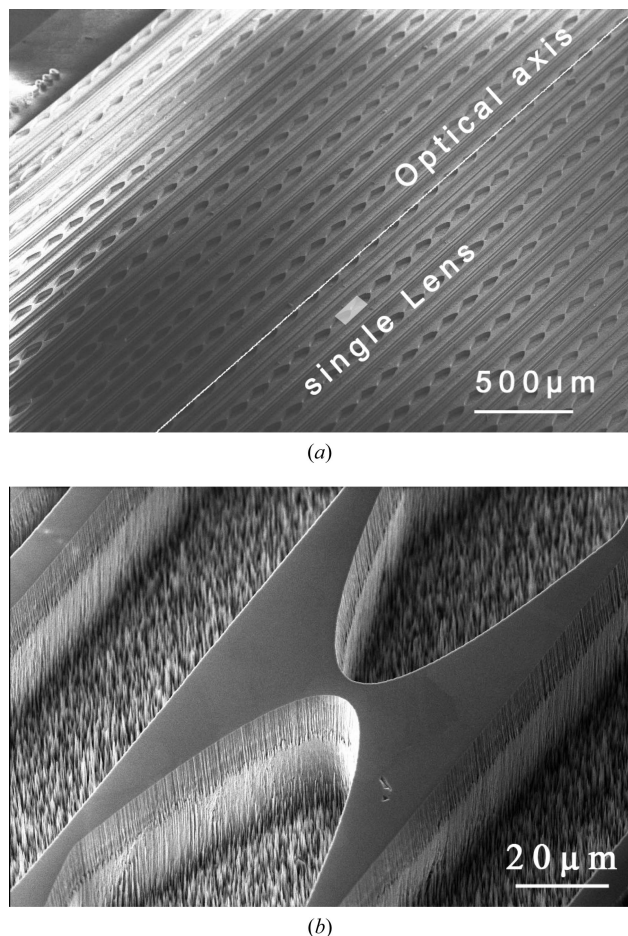


Figure 1 Scanning electron micrograph of the planar nanofocusing refractive lenses made from diamond. An individual bar code is structured into the wafer in between the lenses to ease the process of alignment in the X-ray beam.

focal length is more than three orders of magnitude smaller than the distance to the source, *i.e.* it is about $f = 27$ mm. Therefore the image distance of the source is very slightly larger than the focal length, leading to a source demagnification factor of about 3500. In the case of a perfect lens, the size of the focal spot can be estimated as a convolution of the geometric demagnification of the source and the diffraction-limited resolution d_{diff} , which is defined as (Lengeler *et al.*, 1999)

$$d_{diff} = 0.75\lambda / (2NA), \tag{2}$$

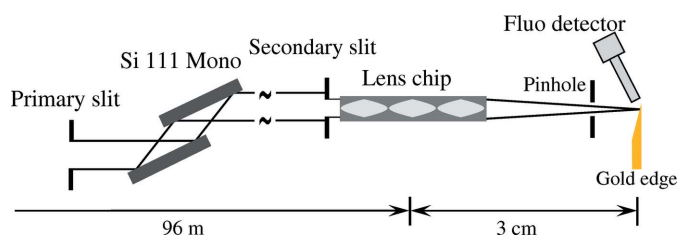


Figure 2 Diamond lens focusing geometry on beamline ID13 at the ESRF.

where $NA = D_{eff}/2f$ is the numerical aperture, D_{eff} is the effective aperture and λ is the wavelength. In our case, for $D_{eff} = 48 \mu\text{m}$, $NA = 8.3 \times 10^{-4}$. Finally, the theoretically expected size of the focal spot for this particular lens is about $d = 27$ nm.

In the first step the diamond lens (with a radius of $6 \mu\text{m}$) was combined with a silicon lens in a crossed geometry to achieve 2D focusing. The radii of curvature of the Si lenses and the distance to the diamond one were chosen such that their foci coincided. The lateral beam profile was characterized in the focus using a gold knife edge that was scanned through the beam (see Fig. 3). The gold knife edge (45 nm gold on an Si_3N_4 membrane) was structured using electron-beam lithography, vacuum deposition of gold and a subsequent lift-off process. The gold edge has a roughness on the 10 nm scale, which is negligible in comparison with the recorded spot size.

The fluorescence radiation of gold was recorded while scanning the knife edge through the focus. A sum of two error functions was fitted to the data. The fitted data (see Fig. 3) reveal a spot size of 360 nm. From Fig. 3 it follows that small parts of the radiation behind the lens were measured outside of the nanobeam, which is easy to see as a shoulder on the right-hand side of the Gaussian. This background is due to aberrations and scattering, but it can be reduced by improving the fabrication process, especially the shape and surface roughness of the lens. We would like to note that scattering by grains of the material has a greater impact than the surface roughness. This effect could be eliminated by using a monocrystalline material for the lens manufacturing. Although the spot size still deviates significantly from the theoretically calculated value (FWHM = 27 nm), this is the smallest spot size generated by a refractive diamond lens manufactured by etching. The discrepancy between the theoretically expected focus size and the measured one has the same origin as the shoulder of the Gaussian and was discussed earlier.

In the second step, in order to estimate the gain increase of intensity in the focal spot due to the use of a diamond lens, we replaced the diamond lens by a Si analogue with similar focal distance, so that we had a set of two Si lenses in the beam. As

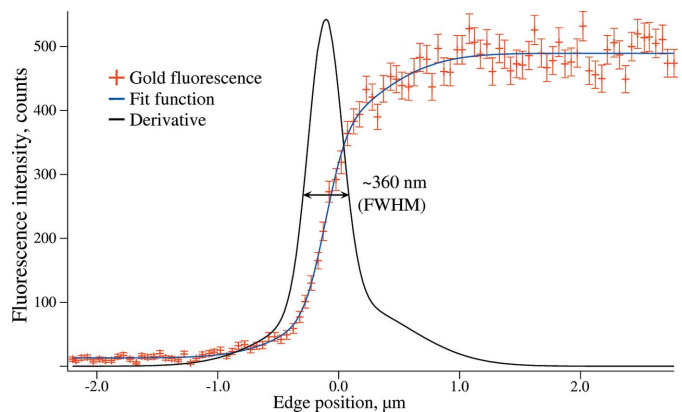


Figure 3 Horizontal scan of a gold edge through the nanobeam. As the edge is scanned through the beam its gold fluorescence radiation is recorded with an energy-dispersive detector. The derivative of the fitted double error function reveals a spot size of approximately 360 nm FWHM.

the result, the photon flux in the beam was significantly reduced: when using a diamond lens for horizontal focusing the photon flux was increased by a factor of 10, so the total photon flux in the beam (diamond and Si lenses) was about $\varphi = 2.1 \times 10^8$ photons s^{-1} . We would like to stress the fact that this number could be larger. The use of two diamond lenses could increase the total flux by another order of magnitude, namely to $\varphi = 2 \times 10^9$ photons s^{-1} . The reason for such a dramatic difference is total transmission: while the diamond lens has a full aperture transmission of 0.44, the Si lens transmission is only 0.04, which is smaller by an order of magnitude.

3. Conclusions

In this article, we have presented a micro-fabrication process for refractive lenses made of diamond. A prototype of a diamond lens was developed, built and successfully tested on beamline ID13 at the ESRF. A spot size of 360 nm (FWHM) at an energy $E = 24.3$ keV was achieved. This is the smallest spot generated by an etched diamond lens. However, at the moment the focus is technologically limited and still far from the ideal diffraction limit. This result inspires us with optimism that the etching technique can provide planar diamond lenses of sufficient quality. On the basis of the experience we have obtained during the manufacture and experimental testing of these lenses, we are planning to optimize the fabrication process in an effort to push the X-ray spot sizes down to the theoretical limit of about 10 nm (Schroer *et al.*, 2003), preserving the highest gain provided by the single-crystalline structure of the material. The improvements will comprise steeper side walls, less roughness, deeper structures and optimized lens design parameters.

Acknowledgements

The authors are grateful to Dennis Brückner for proofreading.

Funding information

This work was supported by the German Ministry of Education and Research (BMBF) under grant No. 05KS7OD1. The

experiments were done as part of the long-term project MI-836 at the ESRF.

References

- Bhardwaj, J. K. & Ashraf, H. (1995). *Proc. SPIE*, **2639**, doi:10.1117/12.221279.
- Fox, O. J. L., Alianelli, L., Malik, A. M., Pape, I., May, P. W. & Sawhney, K. J. S. (2014). *Opt. Express*, **22**, 7657–7668.
- Hettel, R. (2014). *J. Synchrotron Rad.* **21**, 843–855.
- Isakovic, A. F., Stein, A., Warren, J. B., Narayanan, S., Sprung, M., Sandy, A. R. & Evans-Lutterodt, K. (2009). *J. Synchrotron Rad.* **16**, 8–13.
- Kurapova, O., Lengeler, B., Schroer, C. G., Kuchler, M., Gessner, T. & van der Hart, A. (2007). *J. Vac. Sci. Technol. B*, **25**, 1626–1629.
- Lengeler, B., Schroer, C., Tümmler, J., Benner, B., Richwin, M., Snigirev, A., Snigireva, I. & Drakopoulos, M. (1999). *J. Synchrotron Rad.* **6**, 1153–1167.
- Lyubomirskiy, M. & Schroer, C. G. (2016). *Synchrotron Radiat. News*, **29**(4), 21–26.
- Nöhammer, B., Hoszowska, J., Freund, A. K. & David, C. (2003). *J. Synchrotron Rad.* **10**, 168–171.
- Patommel, J., Klare, S., Hoppe, R., Ritter, S., Samberg, D., Wittwer, F., Jahn, A., Richter, K., Wenzel, C., Bartha, J. W., Scholz, M., Seiboth, F., Boesenberg, U., Falkenberg, G. & Schroer, C. G. (2017). *Appl. Phys. Lett.* **110**, 101103.
- Polikarpov, M., Snigireva, I., Morse, J., Yunkin, V., Kuznetsov, S. & Snigirev, A. (2015). *J. Synchrotron Rad.* **22**, 23–28.
- Schroer, C. G., Agapov, I., Brefeld, W., Brinkmann, R., Chae, Y.-C., Chao, H.-C., Eriksson, M., Keil, J., Nuel Gavaldà, X., Röhlberger, R., Seeck, O. H., Sprung, M., Tischer, M., Wanzenberg, R. & Weckert, E. (2018). *J. Synchrotron Rad.* **25**, 1277–1290.
- Schroer, C. G., Kuhlmann, M., Hunger, U. T., Günzler, T. F., Kurapova, O., Feste, S., Frehse, F., Lengeler, B., Drakopoulos, M., Somogyi, A., Simionovici, A. S., Snigirev, A., Snigireva, I., Schug, C. & Schröder, W. H. (2003). *Appl. Phys. Lett.* **82**, 1485–1487.
- Schroer, C. G., Kurapova, O., Patommel, J., Boye, P., Feldkamp, J., Lengeler, B., Burghammer, M., Riekel, C., Vincze, L., van der Hart, A. & Kuchler, M. (2005). *Appl. Phys. Lett.* **87**, 124103.
- Schroer, C. G. & Lengeler, B. (2005). *Phys. Rev. Lett.* **94**, 054802.
- Serebrennikov, D., Clementyev, E., Semenov, A. & Snigirev, A. (2016). *J. Synchrotron Rad.* **23**, 1315–1322.
- Snigirev, A., Kohn, V., Snigireva, I. & Lengeler, B. (1996). *Nature*, **384**, 49–51.
- Snigirev, A., Yunkin, V., Snigireva, I., Di Michiel, M., Drakopoulos, M., Kouznetsov, S., Shabel'nikov, L., Grigoriev, M., Ralchenko, V., Sychoy, I., Hoffmann, M. & Voges, E. (2002). *Proc. SPIE*, **4783**, doi:10.1117/12.451011.
- Tavares, P. F., Leemann, S. C., Sjöström, M. & Andersson, Å. (2014). *J. Synchrotron Rad.* **21**, 862–877.